Size-Differentiated Chemical Characteristics of Asian Paleo Dust: Records from Aeolian Deposition on Chinese Loess Plateau

Feng Wu [a] , Judith C. Chow [a b] , Zhisheng An [a] , John G. Watson [a b] & Junji Cao [a]

[a] State Key Laboratory of Loess and Quaternary Geology, Institute of Earth Environment, Chinese Academy of Sciences, Xi'an, People's Republic of China

[b] Division of Atmospheric Sciences, Desert Research Institute, Reno, NV

PLEASE SCROLL DOWN FOR ARTICLE

Size-Differentiated Chemical Characteristics of Asian Paleo Dust: Records from Aeolian Deposition on Chinese Loess Plateau

Feng Wu
State Key Laboratory of Loess and Quaternary Geology, Institute of Earth Environment, Chinese Academy of Sciences, Xi'an, People's Republic of China

Judith C. Chow
State Key Laboratory of Loess and Quaternary Geology, Institute of Earth Environment, Chinese Academy of Sciences, Xi'an, People's Republic of China; and Division of Atmospheric Sciences, Desert Research Institute, Reno, NV

Zhisheng An
State Key Laboratory of Loess and Quaternary Geology, Institute of Earth Environment, Chinese Academy of Sciences, Xi'an, People's Republic of China

John G. Watson
State Key Laboratory of Loess and Quaternary Geology, Institute of Earth Environment, Chinese Academy of Sciences, Xi'an, People's Republic of China; and Division of Atmospheric Sciences, Desert Research Institute, Reno, NV

Junji Cao
State Key Laboratory of Loess and Quaternary Geology, Institute of Earth Environment, Chinese Academy of Sciences, Xi'an, People's Republic of China

ABSTRACT

The Chinese Loess Plateau (CLP) receives and potentially contributes to Asian dust storms that affect particulate matter (PM) concentrations, visibility, and climate. Loess on the CLP has experienced little weathering effect and is regarded as an ideal record to represent geochemical characteristics of Asian paleo dust. Samples were taken from 2-, 9-, and 15-m depths (representing deposition periods from ~12,000 to ~200,000 yr ago) in the Xi Feng loess profile on the CLP. The samples were resuspended and then sampled through total suspended particulates (TSP), PM_{10}, $PM_{2.5}$, and PM_1 (PM with aerodynamic diameters < ~30, 10, 2.5, and 1 μm, respectively) inlets onto filters for mass, elemental, ionic, and carbon analyses using a Desert Research Institute resuspension chamber. The elements Si, Ca, Al, Fe, K, Mg, water-soluble Ca (Ca^{2+}), organic carbon, and carbonate carbon are the major constituents (>1%) in loess among the four PM fractions (i.e., TSP, PM_{10}, $PM_{2.5}$, and PM_1). Much of Ca is water soluble and corresponds with measures of carbonate, indicating that most of the calcium is in the form of calcium carbonate rather than other calcium minerals. Most of the K is insoluble, indicating that loess can be separated from biomass burning contributions when K^+ is measured. The loess has elemental abundances similar to those of the upper continental crust (UCC) for Mg, Fe, Ti, Mn, V, Cr, and Ni, but substantially different ratios for other elements such as Ca, Co, Cu, As, and Pb. These suggest that the use of UCC as a reference to represent pure or paleo Asian dust needs to be further evaluated. The aerosol samples from the source regions have similar ratios to loess for crustal elements, but substantially different ratios for species from anthropogenic sources (e.g., K, P, V, Cr, Cu, Zn, Ni, and Pb), indicating that the aerosol samples from the geological-source-dominated environment are not a "pure" soil product as compared with loess.

IMPLICATIONS

Precise and representative chemical properties of dust are necessary to quantitatively evaluate the impact of mineral dust on the environment and climate. Efforts to obtain chemical characteristics for Asian paleo dust are valuable for reducing uncertainty in evaluation of the role of Asian dust in climate and environmental change of geologic times as well as during the modern period.

INTRODUCTION

Arid and semi-arid regions in northern and northwestern China are among the largest dust sources in the world. Large amounts of aeolian dust become airborne and are transported toward the east to be deposited in East Asia

and beyond.[1] Asian dust has been detected in deep-sea sediments from the remote Pacific,[2] the atmosphere of the western United States,[3] Greenland ice cores,[4] and Europe.[5] Geological records trace Asian dust to 8–27 million yr before present (B.P.).[6,7] Asian dust alters radiative transfer by scattering and absorbing solar and/or thermal radiation.[8] It is also one of the main sources of water-soluble Fe and P for ocean plankton growth and is expected to accelerate the productivity of marine and terrestrial ecosystems,[9,10] influence the carbon cycle,[11] and change greenhouse gas levels.[11]

Representative chemical characteristics of dust are needed to better evaluate the impact of suspendable dust on the environment and climate.[12,13] The Asia Pacific Regional Aerosol Characterization Experiment (ACE-Asia) and the Chinese Dust Storm Research Project acquired receptor measurements of Asian outflows during dust storms.[14–22] Surface soil from the source regions has been collected, air-dried, size-segregated, and analyzed to obtain size-specific chemical source profiles.[23–25] Fine particle $PM_{2.5}$ (particulate matter [PM] $\leq$ 2.5 μm in aerodynamic diameter) characterization is most useful because $PM_{2.5}$ has long residence times in the atmosphere.[26] Limited measurements exist regarding the characteristics of Asian paleo dust. Surface samples do not tell the whole story, however, because suspendable Asian dust may have differing composition with time.

The loess-paleosol (dusts formed and deposited during geological time that may differ in chemical and physical characteristics from present-day surface dusts) sequence on the Chinese Loess Plateau (CLP) is a product of Asian dust deposition,[27] recording the evolution of Asian paleo dust since the Pliocene ($\sim$22 Ma).[6] As a continental aeolian deposit, loess has experienced little weathering effect and is regarded as an ideal record to represent geochemical characteristics of pure Asian paleo dust.[28] Geochemical studies have been conducted on the loess to distinguish the provenance of Asian paleo dust and decipher East Asian monsoon variability by using different isotopic (e.g., Sm, Nd abundances and elemental ratios [e.g., Zr/Rb, Rb/Sr]).[29–33] However, these previous studies of bulk material have not examined loess properties relevant to suspendable dust in the atmosphere.

This study investigated multiple trace elements, water-soluble ions, and carbon fractions of size-segregated loess (i.e., total suspended particulates [TSP], PM_{10}, $PM_{2.5}$, and PM_1 [PM with aerodynamic diameters < $\sim$30, 10, 2.5, and 1 μm, respectively]) through separation of bulk loess samples by suspension and sampling through size-selective inlets onto filters followed by chemical analyses.[34] Size-differentiated chemical abundances were compared to those from the upper continental crust (UCC) and dust-dominated aerosol in Asian dust source regions.

METHODOLOGY

The CLP is one of the most extensive areas of loess deposition in the world. It spans an area of $\sim$440,000 km^2 predominantly in the provinces of Shanxi, Shaanxi, and Gasnu between 33° north, $-$40° north and 98° east $-$115° east (Figure 1).[1] Xi Feng (35°45' north, 107°49' east), a city in Gansu Province, is located in the central CLP. The loess deposit throughout the region is approximately 130 m thick and contains more than 30 major loess units interbedded with paleosol.[35] Nine loess samples were collected from three loess strata (L1LL1, L1LL2, and L2) of the profile. Loess strata samples were obtained by digging a 20-m-deep well in the upper portion of the CLP, and individual samples were collected with a plastic shovel in
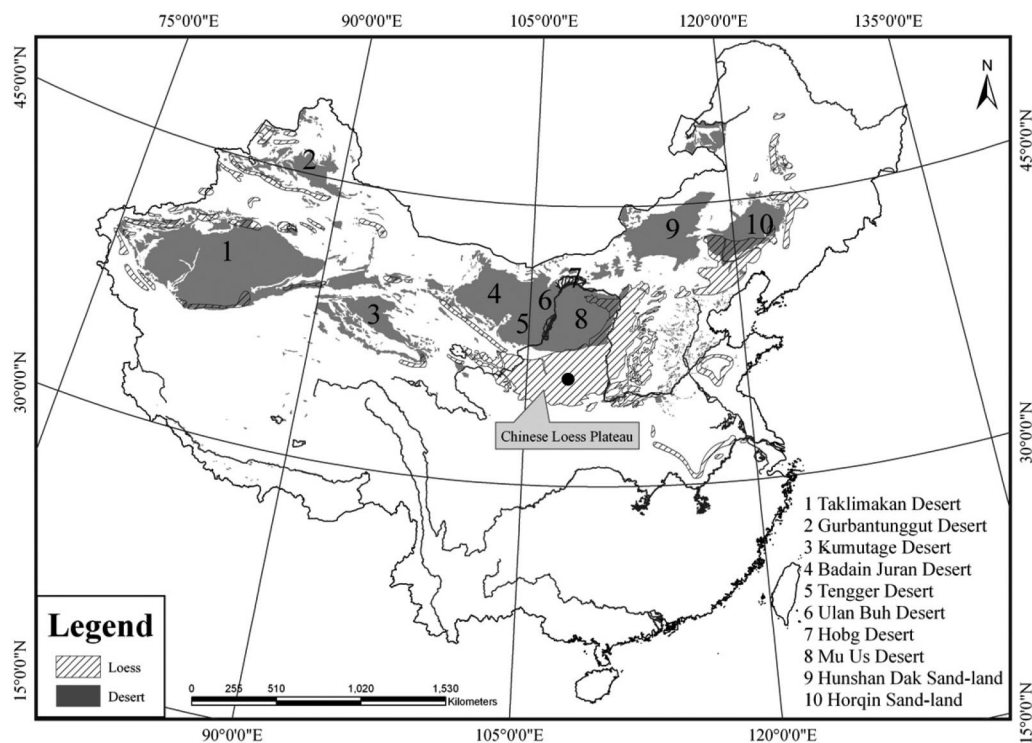
Figure 1. Map of China showing distributions of the CLP as well as major deserts and sand-lands. The loess sampling location is indicated by a black dot.

three typical loess strata. Paleosol samples were not collected because they suffer from strong chemical weathering after deposition and would not represent the original dust characteristics. Age of loess deposit is determined by correlation between the magnetism profiles and the mapping spectral variability in global climate project (SPECMAP) time series.[36] These samples are summarized in Table 1 with their corresponding sampling depth, geological strata, and age of the loess deposit.

Samples were air-dried at 25 °C room temperature for 1 week and sieved through Tyler 30-, 50-, 100-, 200-, and 400-mesh sieves to obtain approximately 5 g of particles with physical diameters less than 38 μm. Approximately 0.1 mg of sieved material was placed in a 250-mL side-arm vacuum flask sealed with a rubber stopper. Air puffs into the flask introduced dust into a resuspension chamber.[34] Clean, filtered laboratory air was drawn into the chamber by the sample flow of 10 L/min through each of six channels equipped with greased PM_{10}, $PM_{2.5}$, and PM_1 impactor inlets. TSP was collected on two channels under the dust cap without specific size segregation. The parallel channels for each size fraction used 47-mm Teflon-membrane filters (Pall Sciences) with 2-mm pore size in channel 1 for mass and subsequent elemental analysis and 47-mm quartz-fiber filters (Whatman Corporation, QM/A) in channel 2 for water-soluble ions, organic carbon (OC), elemental carbon (EC), carbon fractions, and carbonate carbon (CC) analyses. Teflon-membrane filters were periodically weighed during the resuspension process to avoid overloading; optimum loading on Teflon-membrane filters for chemical speciation is 1–3 mg per 47-mm filter.

Teflon-membrane filter samples were equilibrated in a relative humidity (25–30%) and temperature (21.5 ± 0.5 °C) controlled environment before gravimetric analysis to minimize particle volatilization and aerosol liquid water interferences. Filters were weighed on an MT5 microbalance (Mettler-Toledo Ltd.) with a sensitivity of ±0.001 mg. Filters were exposed to a low-level radioactive source (500 pCi of polonium-210) before and during sample weighing to remove static charge. The differences of re-weights for unexposed and exposed filters were below ±0.010 and ±0.015 mg, respectively.

Thirty-nine elements (e.g., Na, Mg, Al, Si, P, S, Cl, K, Ca, Ti, V, Cr, Mn, Fe, Co, Ni, Cu, Zn, Ga, As, Se, Br, Rb, Sr, Y, Zr, Mo, Pd, Ag, Cd, In, Sn, Sb, Ba, Au, Hg, Tl, Pb, and U) were quantified on the Teflon-membrane filters with an Epsilon 5 energy dispersive X-ray fluorescence instrument (ED-XRF; PANalytical).[37] The excitation consisted of a gadolinium (Gd) anode tube, with Ti, Fe, Ge, Zr, Mo, Ag, and barium fluoride (BaF_2) secondary targets. Characteristic X-ray emissions were detected by a solid-state, liquid nitrogen (N_2) cooled Ge detector. Filters were loaded (and unloaded) into the sample holders in a high-efficiency particulate air (HEPA) filter laminar flow hood. One of every 10 samples was reanalyzed, and two MicroMatter multi-element quality assurance (QA) standards (Al, Cl, Ca, Ti, Fe, Se, Y, Mo, Ag, Sn, Ba, and W) were analyzed each day to verify lack of instrument drift.[37]

Fourteen rare earth elements (REEs; La, Ce, Pr, Nd, Sm, Eu, Gd, Tb, Dy, Ho, Er, Tm, Yb, and Lu) were analyzed by inductively coupled plasma–mass spectrometry (ICP-MS, Thermo Elemental, X Series). The entire Teflon filter was sliced into eight pieces, placed in a digestion vessel, and wetted with 0.2 mL of ethanol to counteract its hydrophobic tendencies. Two milliliters of a 2:1 HNO_3:H_2O solution were added, followed by a 1:4 HCl:H_2O solution and 0.1 mL of Hartree–Fock (HF). The HF was needed to dissolve strongly bound mineral oxides in most geological samples. The capped digestion vessel was placed in a hot block for 90 min, cooled, and brought to 50 mL total volume with distilled-deionized water (DDW). The capped vessels were stored overnight with the cap side down before analysis. The ICP-MS was equipped with a concentric nebulizer with a cooled (2–3 °C) spray chamber that minimized oxide formation[38,39] and a collision cell chamber to reduce polyatomic interferences.[40–42] The ICP-MS was optimized and calibrated daily for the elements of interest and maintained less than 2% oxide formation and less than 2% double-charged ions. A calibration curve from 0.001 to 500 μg/L was plotted each day. External standards, reagent blanks, and filter blanks were analyzed each day. Replicates, spikes, and QA standards were run at a rate of 10%.

Half of the quartz-fiber filter was extracted in DDW and analyzed for water-soluble chloride (Cl^-), nitrate (NO_3^-), and sulfate (SO_4^{2-}) by ion chromatography[43]; for water-soluble sodium (Na^+), potassium (K^+), and calcium (Ca^{2+}) by atomic absorption spectrophotometry (AAS); and for water-soluble ammonia (NH_4^+) by automated colorimetry (AC). A 0.5-cm^2 punch from the remaining half filters was analyzed for eight carbon fractions following the Interagency Monitoring of Protected Visual Environments (IMPROVE) thermal/optical reflectance (TOR) protocol.[44–47] This produced four temperature-specific OC fractions (OC1, OC2, OC3, and OC4 at 120, 250, 450, and 550 °C, respectively, in a 100% helium [He] atmosphere), a pyrolyzed carbon fraction (OP; determined when reflected laser light attained its original intensity after oxygen [O_2] was added to the analysis atmosphere), and three EC fractions (EC1, EC2, and EC3 at 550, 700,

Table 1. Description of loess samples collected from the Xi Feng loess profile at the CLP.

Strata[a]	Sample ID	Depth from Surface (m)	Age of Loess Deposit (1000 yr B.P.)[b]
L1LL1	ZJC-L1–0	2.2	ca. 12.5 − 28.2
	ZJC-L1–1	2.4	
	ZJC-L1–2	2.6	
L1LL2	ZJC-L1–34	9	ca. 65 − 73
	ZJC-L1–35	9.2	
	ZJC-L1–36	9.4	
L2	ZJC-L2–5	14.7	ca. 125 − 198
	ZLC-L2–6	15.1	
	ZLC-L2–8	15.5	

Notes: [a]L1LL1 and L1LL2 represent two loess horizons in Malan loess (L1) deposited during the last glacial period; L2 represents loess deposited during the penultimate glacial periods. [b]Age of loess deposit is determined by correlation between the magnetism profiles and the SPECMAP time series.[36] Paleosol samples (represented by gaps in deposit age) were not collected because strong chemical weathering after deposition means they are non-representative of the original characteristics of paleo dust.

and 800 °C, respectively, in a 98% H3/2% O_2 atmosphere). IMPROVE OC is defined as OC1 + OC2 + OC3 + OC4 + OP, and EC is defined as EC1 + EC2 + EC3 − OP. The CC abundance was determined by acidification of the sample with HCl before thermal/optical analysis with subsequent detection of evolved carbon dioxide (CO_2).[48] Mass fractions (abundances) were calculated for each measured component after blank subtraction. Uncertainties for individual samples were determined by error propagation of precisions derived from replicate measurements and standard deviations of filter blanks.[49]

RESULTS AND DISCUSSION
Chemical Characteristics for Different Size Fractions

Table 2 compares chemical abundances for TSP, PM_{10}, $PM_{2.5}$, and PM_1 size fractions for the three sampled strata; also listed are composite source profiles for CLP surface dust from Cao's earlier paper.[24] Six major crustal elements (Si, Ca, Al, Fe, K, and Mg) show abundances (>1% with low variability). Ti and Mn abundances are in the range of 0.1–1%. Because O_2 was not measured, the IMPROVE formula[50] was used to estimate mineral mass as the weighted sum of aluminum, silicon, calcium, iron, and titanium oxides ($[Soil] = 1.94 \times [Ti] + 2.49 \times [Si] + 2.42 \times [Fe] + 1.63 \times [Ca] + 2.2 \times [Al]$). This reconstructed mass accounts for 80–90% of total measured mass. Si is the most abundant species, but it shows the greatest variation (12–24%) among size fractions: 20–24% in TSP, 12–13% in PM_{10}, and 13–15% in $PM_{2.5}$ and PM_1. Al, Fe, K, and Mg are more abundant in the $PM_{2.5}$ and PM_1 size fractions than in the TSP fraction. $PM_{2.5}$ Al and Fe abundances are 70 and 40% higher than corresponding levels in TSP, respectively. $PM_{2.5}$ and PM_1 Ti and Mn abundances are 30% higher than those in TSP. REE abundances are higher in $PM_{2.5}$ and PM_1 than in TSP. La abundance ranges from 18 to 22 parts per million by weight (ppmw) in TSP, which increases to 31–42 ppmw in PM_1. PM Ca abundances are less variable, ranging from 10 to 15%. Many trace element abundances are close or lower than their variability and show no consistent relationship to the size fraction.

Cations (K^+, Ca^{2+}, Na^+, NH_4^+) and anions (Cl^-, NO_3^-, and SO_4^{2-}) account for 9–13% of PM mass. Ca^{2+} (8–13%) is the most abundant ion, constituting 90% of total water-soluble ions. The ratios of Ca^{2+}/Ca range from 0.7 to 1, indicating that most Ca is water-soluble. This indicates that the Ca multiplier in the IMPROVE formula, which assumes Ca, is probably incorrect because calcium oxide (CaO) is largely insoluble. A large Ca^{2+} abundance is consistent with the content of modern surface dust from the Zhenbeitai (ZBT) station in northern CLP (Figure 1).[15] Water-soluble K^+ is the second most abundant ion (0.1–0.4%), but this is much lower than the Ca^{2+} abundance. K^+ abundances increase as the size fraction decreases, constituting 0.10–0.17% of TSP and 0.26–0.37% in PM_1. Total K is 5–25 times the K^+ abundance for all samples, indicating that most K is not water-soluble. Because the K abundance in biomass burning emissions is nearly all K^+,[51–53] Asian dust contributions can be separated from vegetative burning using these markers. The remaining ionic species abundances are low, with 0.06–0.15% for SO_4^{2-}, 0.02–0.08% for Na^+, 0.02–0.05% for NH_4^+, and 0.03–0.14% for NO_3. Cl^- is enriched for the larger size fractions, with TSP abundances of 0.08–0.15% and PM_1 abundances of 0.04–0.08%.

Total carbon (TC = OC + EC + CC) accounts for 4–7% of measured mass. Average abundances of CC in PM loess are 2–5%, constituting 50–80% of TC. Figure 2 shows good correlation (0.75 < r < 0.95) between CO_3^{2-}-C and Ca^{2+} in all size fractions, with mass ratios of CO_3^{2-}-C/Ca^{2+} (0.2–0.29) close to the $CaCO_3$ stoichiometric ratio [C(12)/Ca (40) = 0.3]. $CaCO_3$, in one of its many mineral forms, is an important component in surface as well as buried paleosols, similar to modern dust over the CLP.[54]

OC constitutes 1.2–3.4% of mass, with OC/TC ratios between 0.25 and 0.5. The main component of OC is high-temperature (450 °C) OC3, accounting for 30–50% of OC in all size fractions. The EC abundance is mostly below the minimum detection limits. There is little or no variation in the abundances of all carbon fractions among the four size fractions.

Chemical abundances of loess PM from different depths are similar, indicating that Asian dusts share similar chemical profiles at least in the last two glacial and interglacial cycles. This may be attributed to the relative stability of the source of Asian paleo dust.

Composite profiles for nine loess samples, calculated by averaging the chemical abundances of individual profiles in each size fraction, are applied to comparisons below.

Comparisons with UCC

Elemental abundances from sampled loess were compared with the composite reference values for the Earth's UCC[55] in Figure 3. UCC abundances represent the average elemental composition of the Earth's surface and were usually used as a reference for pure or paleo dust. Suspendable loess has several abundances that are similar to those of the UCC, as indicated by ratios close to unity in Figure 3. Most notable are Mg, Fe, Ti, Mn, V, Cr, and Ni, which have ratios of 1–2. These elemental abundances would not be useful for distinguishing CLP Asian dust contributions from other dust sources.

Positive deviations from unity of 2–6 are evident for Ca, Co, Cu, As, and Pb, whereas negative deviations are evident for Na, Si, K, P, Br, Rb, Sr, and Zr. Average abundances of Mg, K, Rb, Sr, Zr, and Ba are all 50–90% of that in UCC; Si is 30–80% of that in UCC; and Na and P are 10–20% of those in UCC. The loess Al abundance is similar to that of UCC for the $PM_{2.5}$ and PM_1 sizes, but it is lower for the TSP and PM_{10} fractions. The Y abundance in loess is similar to that of UCC for TSP and PM_{10}, but it is higher for $PM_{2.5}$ and PM_1. Light REE abundances (La, Ce, Pr, and Nd) in UCC are similar to those of loess PM_{10}, whereas heavy REE abundances (Ho, Er, Tm, Yb, and Lu) in loess are similar to those of UCC for $PM_{2.5}$ and PM_1. The differences of elemental abundances between loess PM and UCC reflect the petrography in the source regions of Asian dust, which is of typical abundances in $CaCO_3$[56] and does not exhibit the same composition as the global

Table 2. Mass fractions in each layer for TSP, PM_{10}, $PM_{2.5}$, and PM_1 size fractions.

Species[b]	Methods[c]	Unit	L1L1 (n = 3) TSP	PM10	PM2.5	PM1	L1L2 (n = 3) TSP	PM10	PM2.5	PM1	L2 (n = 3) TSP	PM10	PM2.5	PM1	Surface Soil (n = 15)[24] TSP	PM10	PM2.5	PM1
Cl^-	IC	%	0.08 ± 0.04	0.12 ± 0.07	0.09 ± 0.09	0.08 ± 0.11	0.15 ± 0.11	0.12 ± 0.08	0.05 ± 0.08	0.04 ± 0.10	0.12 ± 0.09	0.12 ± 0.08	0.03 ± 0.11	0.05 ± 0.21	0.14	0.26	0.37	0.50
NO_3^-	IC	%	0.03 ± 0.07	0.08 ± 0.07	0.10 ± 0.10	0.10 ± 0.11	0.07 ± 0.11	0.09 ± 0.08	0.06 ± 0.08	0.03 ± 0.10	0.08 ± 0.09	0.04 ± 0.08	0.08 ± 0.11	0.14 ± 0.21	0.00	0.00	0.00	0.00
SO_4^{2-}	IC	%	0.06 ± 0.04	0.10 ± 0.07	0.11 ± 0.09	0.14 ± 0.11	0.15 ± 0.11	0.09 ± 0.08	0.09 ± 0.09	0.10 ± 0.11	0.12 ± 0.09	0.11 ± 0.08	0.11 ± 0.11	0.15 ± 0.21	0.04	0.06	0.04	0.04
NH_4^+	AC	%	0.02 ± 0.02	0.04 ± 0.04	0.05 ± 0.06	0.05 ± 0.09	0.03 ± 0.05	0.02 ± 0.04	0.02 ± 0.06	0.03 ± 0.08	0.04 ± 0.05	0.04 ± 0.04	0.04 ± 0.09	0.06 ± 0.17	0.05	0.12	0.21	0.22
Na^+	AAS	%	0.02 ± 0.01	0.05 ± 0.01	0.08 ± 0.05	0.07 ± 0.08	0.04 ± 0.01	0.03 ± 0.04	0.07 ± 0.06	0.06 ± 0.08	0.04 ± 0.01	0.08 ± 0.03	0.05 ± 0.09	0.06 ± 0.16	0.04	0.07	0.13	0.12
K^+	AAS	%	0.10 ± 0.02	0.19 ± 0.03	0.46 ± 0.08	0.37 ± 0.10	0.17 ± 0.03	0.17 ± 0.03	0.41 ± 0.08	0.31 ± 0.10	0.12 ± 0.02	0.10 ± 0.03	0.26 ± 0.09	0.26 ± 0.17	0.09	0.15	0.31	0.26
Ca^{2+}	AAS	%	8.66 ± 0.90	12.18 ± 1.20	10.33 ± 1.03	12.63 ± 1.75	13.07 ± 1.21	11.80 ± 1.07	12.15 ± 1.40	9.69 ± 1.53	13.28 ± 1.16	11.00 ± 1.07	9.27 ± 1.22	8.90 ± 1.18	NA	NA	NA	NA
OC1	TOR	%	0.04 ± 0.07	0.01 ± 0.10	0.07 ± 0.37	0.09 ± 0.60	0.00 ± 0.11	0.06 ± 0.14	0.04 ± 0.41	0.10 ± 0.58	0.05 ± 0.12	0.03 ± 0.17	0.02 ± 0.60	0.15 ± 1.17	0.01	0.02	0.09	0.00
OC2	TOR	%	0.25 ± 0.12	0.35 ± 0.18	0.48 ± 0.42	0.25 ± 0.62	0.34 ± 0.22	0.33 ± 0.21	0.26 ± 0.44	0.39 ± 0.61	0.45 ± 0.22	0.32 ± 0.23	0.28 ± 0.62	0.29 ± 1.18	0.15	0.33	0.51	0.09
OC3	TOR	%	0.47 ± 0.25	0.91 ± 0.43	1.53 ± 0.69	0.57 ± 0.76	1.08 ± 0.64	1.34 ± 0.54	0.66 ± 0.59	0.83 ± 0.76	1.05 ± 0.55	0.80 ± 0.48	0.82 ± 0.78	0.87 ± 1.44	0.49	0.94	1.44	1.07
OC4	TOR	%	0.24 ± 0.13	0.46 ± 0.24	0.83 ± 0.50	0.40 ± 0.62	0.29 ± 0.25	0.47 ± 0.27	0.39 ± 0.45	0.67 ± 0.64	0.41 ± 0.26	0.36 ± 0.26	0.73 ± 0.67	0.71 ± 1.21	0.32	0.73	1.19	0.81
OP	TOR	%	0.32 ± 0.19	0.24 ± 0.22	0.79 ± 0.65	0.36 ± 0.68	0.52 ± 0.36	1.04 ± 0.70	0.37 ± 0.50	0.70 ± 0.71	0.00 ± 0.15	0.18 ± 0.25	0.14 ± 0.61	0.00 ± 1.15	0.48	1.11	0.73	0.73
OC	TOR	%	1.29 ± 0.54	1.91 ± 0.84	3.44 ± 1.72	1.22 ± 1.92	2.16 ± 1.12	3.15 ± 1.26	1.36 ± 1.41	2.28 ± 1.96	1.90 ± 0.95	1.55 ± 0.92	1.55 ± 1.93	1.35 ± 3.51	1.44	3.13	3.96	2.70
EC1	TOR	%	0.21 ± 0.08	0.67 ± 0.24	1.13 ± 0.40	0.51 ± 0.25	0.44 ± 0.19	1.02 ± 0.34	0.39 ± 0.18	0.86 ± 0.35	0.31 ± 0.15	0.30 ± 0.13	0.65 ± 0.28	0.64 ± 0.40	0.33	0.75	1.28	0.53
EC2	TOR	%	0.11 ± 0.11	0.25 ± 0.21	0.29 ± 0.26	0.13 ± 0.21	0.12 ± 0.17	0.23 ± 0.25	0.14 ± 0.18	0.34 ± 0.31	0.11 ± 0.16	0.05 ± 0.13	0.33 ± 0.37	0.34 ± 0.51	0.14	0.31	0.42	0.20
EC3	TOR	%	0.00 ± 0.02	0.09 ± 0.10	0.03 ± 0.10	0.00 ± 0.14	0.01 ± 0.05	0.01 ± 0.04	0.00 ± 0.10	0.06 ± 0.15	0.15 ± 0.17	0.00 ± 0.05	0.30 ± 0.34	0.27 ± 0.41	0.04	0.07	0.02	0.11
EC	TOR	%	0.00 ± 0.24	0.76 ± 0.40	0.66 ± 0.84	0.28 ± 0.85	0.04 ± 0.44	0.23 ± 0.81	0.16 ± 0.63	0.55 ± 0.93	0.57 ± 0.32	0.17 ± 0.33	1.14 ± 0.93	1.25 ± 1.59	0.02	0.03	0.99	0.12
CC	TOR	%	4.21 ± 0.99	4.60 ± 1.16	3.40 ± 0.96	3.22 ± 1.05	4.62 ± 1.37	3.66 ± 1.02	3.96 ± 1.06	3.63 ± 1.09	4.63 ± 1.28	3.65 ± 1.03	2.91 ± 0.97	2.71 ± 1.46	1.77	3.38	2.45	2.13
TC	TOR	%	5.49 ± 1.13	7.25 ± 1.54	7.39 ± 2.17	4.53 ± 2.72	6.80 ± 1.65	7.00 ± 1.52	5.34 ± 2.10	6.27 ± 2.78	7.08 ± 1.56	5.32 ± 1.39	5.40 ± 2.78	4.75 ± 4.94	1.46	3.16	4.95	2.81
Na	XRF	%	0.35 ± 0.08	0.38 ± 0.12	0.43 ± 0.16	0.53 ± 0.17	0.28 ± 0.16	0.60 ± 0.16	0.65 ± 0.18	0.44 ± 0.16	0.25 ± 0.14	0.57 ± 0.16	0.49 ± 0.19	0.38 ± 0.29	0.16	0.42	0.27	0.67
Mg	XRF	%	1.15 ± 0.14	1.71 ± 0.22	2.46 ± 0.31	2.37 ± 0.35	1.54 ± 0.24	2.01 ± 0.25	2.15 ± 0.29	2.24 ± 0.33	1.27 ± 0.20	1.81 ± 0.25	2.29 ± 0.36	2.34 ± 0.44	0.17	0.35	0.48	0.42
Al	XRF	%	4.37 ± 0.44	6.06 ± 0.56	8.01 ± 0.78	8.09 ± 1.02	5.37 ± 0.47	6.79 ± 0.60	7.47 ± 0.80	7.46 ± 0.94	4.63 ± 0.60	6.34 ± 0.60	8.16 ± 1.03	8.08 ± 1.05	5.58	9.14	5.02	4.90
Si	XRF	%	20.09 ± 11.2	12.32 ± 1.14	14.28 ± 1.40	14.99 ± 1.89	24.84 ± 13.7	13.68 ± 1.21	13.17 ± 1.43	14.33 ± 1.81	20.62 ± 11.4	12.94 ± 1.23	14.68 ± 1.86	15.17 ± 1.96	17.54	27.41	14.58	14.27
K	XRF	%	1.79 ± 0.63	2.33 ± 0.80	2.27 ± 0.21	2.34 ± 0.29	2.26 ± 0.78	2.69 ± 0.93	2.19 ± 0.23	2.30 ± 0.28	1.80 ± 0.62	2.48 ± 0.86	2.33 ± 0.29	2.31 ± 0.29	1.72	2.52	2.30	2.17
Ca	XRF	%	10.41 ± 3.13	15.33 ± 4.49	12.97 ± 1.24	14.33 ± 1.80	11.03 ± 3.22	13.88 ± 4.06	11.98 ± 1.28	14.05 ± 1.76	10.86 ± 3.24	14.84 ± 4.43	12.03 ± 1.53	13.38 ± 1.78	6.78	9.83	9.74	9.99
Fe	XRF	%	3.56 ± 0.35	4.38 ± 0.39	5.22 ± 0.49	5.46 ± 0.68	4.29 ± 0.36	4.84 ± 0.41	4.83 ± 0.51	5.33 ± 0.66	3.41 ± 0.28	4.46 ± 0.41	5.24 ± 0.65	5.29 ± 0.67	3.12	4.40	5.01	4.72
Ti	XRF	%	0.31 ± 0.03	0.36 ± 0.03	0.40 ± 0.07	0.42 ± 0.09	0.36 ± 0.03	0.38 ± 0.04	0.35 ± 0.07	0.40 ± 0.09	0.28 ± 0.03	0.37 ± 0.04	0.40 ± 0.10	0.41 ± 0.16	0.30	0.41	0.41	0.40
Mn	XRF	%	0.09 ± 0.01	0.12 ± 0.02	0.12 ± 0.02	0.14 ± 0.03	0.10 ± 0.02	0.11 ± 0.02	0.11 ± 0.02	0.12 ± 0.03	0.09 ± 0.02	0.12 ± 0.02	0.12 ± 0.03	0.13 ± 0.04	0.07	0.11	0.13	0.12
P	XRF	ppm	68 ± 39	36 ± 74	195 ± 106	40 ± 103	94 ± 102	101 ± 88	239 ± 105	227 ± 107	66 ± 90	108 ± 94	0 ± 124	104 ± 205	328	509	550	761
S	XRF	ppm	115 ± 17	152 ± 29	209 ± 58	147 ± 69	98 ± 30	131 ± 30	172 ± 60	139 ± 67	95 ± 28	155 ± 35	122 ± 80	85 ± 130	295	509	448	503
Cl	XRF	ppm	185 ± 39	310 ± 69	408 ± 155	376 ± 195	88 ± 79	145 ± 74	92 ± 162	115 ± 186	95 ± 71	297 ± 96	97 ± 225	171 ± 371	587	757	646	749
V	XRF	ppm	45 ± 23	87 ± 53	80 ± 262	62 ± 354	41 ± 42	120 ± 64	63 ± 295	80 ± 349	68 ± 42	53 ± 106	95 ± 422	81 ± 697	107	161	173	178
Cr	XRF	ppm	51 ± 32	61 ± 61	62 ± 102	69 ± 116	56 ± 82	46 ± 72	102 ± 105	69 ± 114	48 ± 74	62 ± 79	70 ± 139	60 ± 227	71	95	143	120
Co	XRF	ppm	65 ± 17	43 ± 30	75 ± 43	57 ± 46	76 ± 40	74 ± 35	46 ± 43	72 ± 45	39 ± 36	72 ± 37	36 ± 54	58 ± 89	60	86	85	75
Ni	XRF	ppm	32 ± 24	27 ± 46	21 ± 60	52 ± 59	17 ± 63	24 ± 54	31 ± 58	32 ± 57	27 ± 55	25 ± 56	20 ± 70	24 ± 116	32	48	63	56
Cu	XRF	ppm	86 ± 27	59 ± 36	56 ± 50	49 ± 51	149 ± 52	108 ± 44	98 ± 50	55 ± 49	44 ± 44	48 ± 44	45 ± 61	95 ± 100	31	50	68	58
Zn	XRF	ppm	25 ± 76	120 ± 50	142 ± 66	157 ± 65	102 ± 67	140 ± 60	131 ± 60	142 ± 63	82 ± 59	98 ± 60	100 ± 74	222 ± 124	97	163	182	156
Ga	XRF	ppm	0 ± 20	38 ± 146	75 ± 186	15 ± 173	61 ± 200	16 ± 172	16 ± 176	46 ± 171	0 ± 177	65 ± 180	36 ± 207	51 ± 342	0	1	5	74
As	XRF	ppm	0 ± 17	8 ± 39	18 ± 65	4 ± 74	0 ± 53	28 ± 46	0 ± 67	8 ± 73	14 ± 47	0 ± 50	13 ± 89	8 ± 147	15	28	46	96
Se	XRF	ppm	0 ± 20	0 ± 33	0 ± 48	0 ± 50	0 ± 46	0 ± 40	0 ± 47	0 ± 49	0 ± 41	0 ± 42	0 ± 59	0 ± 98	2	2	9	9
Br	XRF	ppm	65 ± 20	26 ± 38	41 ± 52	19 ± 52	20 ± 52	25 ± 45	50 ± 51	43 ± 51	3 ± 46	7 ± 47	12 ± 61	46 ± 102	3	2	3	3
Rb	XRF	ppm	277 ± 53	367 ± 93	116 ± 51	126 ± 52	110 ± 50	77 ± 43	67 ± 49	139 ± 53	55 ± 43	70 ± 45	107 ± 61	44 ± 98	79	108	107	109
Sr	XRF	ppm	20 ± 28	13 ± 55	319 ± 114	372 ± 113	180 ± 118	212 ± 102	227 ± 106	299 ± 107	337 ± 108	332 ± 111	343 ± 129	377 ± 205	166	232	293	246
Y	XRF	ppm	116 ± 62	15 ± 74	15 ± 74	74 ± 73	6 ± 76	22 ± 65	54 ± 72	65 ± 72	42 ± 67	22 ± 68	85 ± 88	52 ± 144	24	39	51	35
Zr	XRF	ppm	7 ± 63	163 ± 117	123 ± 148	133 ± 139	110 ± 158	47 ± 136	122 ± 140	189 ± 139	113 ± 140	169 ± 143	164 ± 166	215 ± 273	86	112	126	92
Mo	XRF	ppm	13 ± 87	15 ± 123	0 ± 163	29 ± 160	48 ± 169	40 ± 145	28 ± 158	72 ± 158	4 ± 148	38 ± 151	0 ± 190	48 ± 315	10	12	51	11
Pd	XRF	ppm	30 ± 69	9 ± 169	68 ± 280	22 ± 315	9 ± 227	15 ± 200	41 ± 286	64 ± 311	19 ± 202	13 ± 215	55 ± 376	0 ± 620	5	11	59	7
Ag	XRF	ppm	30 ± 69	11 ± 133	36 ± 275	100 ± 337	82 ± 177	58 ± 159	72 ± 294	37 ± 332	132 ± 158	16 ± 180	108 ± 402	157 ± 664	8	11	16	47

Table 2. (Cont.)

Species[b]	Analysis Methods[c]	Unit	L1L1 (n = 3)				L1L2 (n = 3)				L2 (n = 3)				Surface Soil (n = 15)[24]			
			TSP	PM$_{10}$	PM$_{2.5}$	PM$_1$	TSP	PM$_{10}$	PM$_{2.5}$	PM$_1$	TSP	PM$_{10}$	PM$_{2.5}$	PM$_1$	TSP	PM$_{10}$	PM$_{2.5}$	PM$_1$
Cd	XRF	ppm	22 ± 76	59 ± 149	9 ± 297	97 ± 361	38 ± 196	5 ± 175	120 ± 317	16 ± 355	47 ± 174	79 ± 197	85 ± 431	8 ± 710	16	20	9	149
In	XRF	ppm	19 ± 74	1 ± 146	57 ± 317	42 ± 393	92 ± 192	58 ± 172	82 ± 341	75 ± 387	138 ± 171	50 ± 198	106 ± 469	46 ± 774	12	23	34	37
Sn	XRF	ppm	54 ± 90	21 ± 176	19 ± 403	0 ± 505	27 ± 227	15 ± 207	29 ± 435	0 ± 497	0 ± 203	0 ± 243	0 ± 601	0 ± 994	20	12	82	31
Sb	XRF	ppm	0 ± 83	2 ± 164	65 ± 432	60 ± 553	0 ± 208	29 ± 195	44 ± 472	25 ± 545	0 ± 187	0 ± 238	45 ± 659	17 ± 1088	4	5	6	3
Ba	XRF	ppm	507 ± 226	375 ± 446	310 ± 1448	726 ± 1906	603 ± 530	614 ± 532	592 ± 1608	396 ± 1877	103 ± 474	620 ± 706	805 ± 2271	425 ± 3748	239	298	785	290
Au	XRF	ppm	23 ± 86	24 ± 165	0 ± 215	25 ± 206	38 ± 226	46 ± 195	51 ± 206	19 ± 203	2 ± 199	34 ± 203	18 ± 245	0 ± 405	3	1	8	53
Hg	XRF	ppm	0 ± 32	0 ± 63	0 ± 94	0 ± 101	0 ± 85	7 ± 74	0 ± 94	0 ± 99	0 ± 76	0 ± 79	0 ± 120	0 ± 198	6	10	39	22
Tl	XRF	ppm	0 ± 66	0 ± 127	0 ± 166	26 ± 159	32 ± 173	7 ± 150	14 ± 158	0 ± 156	0 ± 154	0 ± 156	20 ± 189	35 ± 312	5	8	5	22
Pb	XRF	ppm	45 ± 63	41 ± 123	59 ± 166	47 ± 164	80 ± 168	67 ± 145	78 ± 161	94 ± 161	55 ± 148	38 ± 151	26 ± 195	111 ± 323	45	69	221	65
U	XRF	ppm	47 ± 84	50 ± 163	17 ± 208	68 ± 195	12 ± 223	112 ± 193	50 ± 197	100 ± 193	26 ± 197	89 ± 199	3 ± 232	32 ± 384	4	4	16	19
La	ICP-MS	ppm	18.49 ± 0.86	30.74 ± 1.31	34.50 ± 1.72	33.93 ± 2.01	21.83 ± 1.24	29.02 ± 1.54	31.49 ± 1.84	31.80 ± 1.64	22.61 ± 1.34	27.46 ± 1.50	29.42 ± 1.35	42.11 ± 2.47	NA	NA	NA	NA
Ce	ICP-MS	ppm	36.59 ± 1.40	60.02 ± 2.15	67.25 ± 2.87	65.70 ± 2.46	43.83 ± 1.62	57.77 ± 2.12	62.43 ± 2.26	62.56 ± 2.15	43.68 ± 2.30	53.28 ± 1.58	56.88 ± 2.52	81.34 ± 3.30	NA	NA	NA	NA
Pr	ICP-MS	ppm	4.43 ± 0.24	7.31 ± 0.27	8.18 ± 0.32	8.12 ± 0.44	5.29 ± 0.30	7.04 ± 0.60	7.62 ± 0.36	7.56 ± 0.44	5.06 ± 0.25	6.28 ± 0.29	6.84 ± 0.46	9.65 ± 0.62	NA	NA	NA	NA
Nd	ICP-MS	ppm	17.01 ± 0.73	28.00 ± 2.00	31.61 ± 2.65	30.98 ± 2.55	20.41 ± 1.73	27.06 ± 2.35	29.63 ± 1.84	29.82 ± 2.24	20.21 ± 1.44	24.96 ± 1.79	26.56 ± 1.67	38.77 ± 3.39	NA	NA	NA	NA
Sm	ICP-MS	ppm	3.31 ± 0.34	5.58 ± 0.57	6.40 ± 0.65	6.24 ± 0.58	4.12 ± 1.09	5.50 ± 0.64	5.98 ± 0.65	6.21 ± 0.56	4.03 ± 0.67	4.94 ± 0.44	5.57 ± 0.66	7.64 ± 0.66	NA	NA	NA	NA
Eu	ICP-MS	ppm	0.69 ± 0.20	1.19 ± 0.41	1.30 ± 0.46	1.29 ± 0.41	0.79 ± 0.33	1.10 ± 0.39	1.25 ± 0.43	1.28 ± 0.21	0.84 ± 0.13	1.01 ± 0.14	1.32 ± 0.45	1.63 ± 0.21	NA	NA	NA	NA
Gd	ICP-MS	ppm	3.24 ± 0.40	5.44 ± 0.63	6.44 ± 0.89	6.26 ± 1.29	4.02 ± 0.84	5.49 ± 0.88	6.22 ± 0.85	6.33 ± 0.82	4.21 ± 0.81	5.05 ± 0.68	6.02 ± 1.20	8.34 ± 1.95	NA	NA	NA	NA
Tb	ICP-MS	ppm	0.42 ± 0.03	0.75 ± 0.13	0.86 ± 0.10	0.81 ± 0.08	0.51 ± 0.12	0.71 ± 0.18	0.81 ± 0.20	0.87 ± 0.21	0.54 ± 0.13	0.68 ± 0.15	0.87 ± 0.23	1.07 ± 0.14	NA	NA	NA	NA
Dy	ICP-MS	ppm	2.20 ± 0.15	3.79 ± 0.20	4.55 ± 0.33	4.38 ± 0.33	2.75 ± 0.29	3.81 ± 0.48	4.42 ± 0.63	4.46 ± 0.29	2.64 ± 0.36	3.34 ± 0.49	3.91 ± 0.49	5.45 ± 0.48	NA	NA	NA	NA
Ho	ICP-MS	ppm	0.39 ± 0.04	0.70 ± 0.11	0.83 ± 0.09	0.78 ± 0.08	0.51 ± 0.12	0.68 ± 0.07	0.78 ± 0.06	0.83 ± 0.15	0.47 ± 0.06	0.62 ± 0.05	0.80 ± 0.24	0.99 ± 0.14	NA	NA	NA	NA
Er	ICP-MS	ppm	1.11 ± 0.15	1.94 ± 0.20	2.39 ± 0.28	2.24 ± 0.22	1.44 ± 0.23	1.96 ± 0.30	2.26 ± 0.33	2.32 ± 0.33	1.38 ± 0.21	1.75 ± 0.30	2.09 ± 0.56	2.81 ± 0.46	NA	NA	NA	NA
Tm	ICP-MS	ppm	0.15 ± 0.03	0.30 ± 0.11	0.33 ± 0.11	0.29 ± 0.08	0.17 ± 0.04	0.28 ± 0.10	0.30 ± 0.07	0.30 ± 0.08	0.19 ± 0.06	0.24 ± 0.06	0.43 ± 0.33	0.40 ± 0.14	NA	NA	NA	NA
Yb	ICP-MS	ppm	1.00 ± 0.14	1.70 ± 0.29	2.08 ± 0.29	1.95 ± 0.34	1.22 ± 0.28	1.68 ± 0.38	2.03 ± 0.63	1.97 ± 0.37	1.20 ± 0.42	1.52 ± 0.32	2.01 ± 0.76	2.55 ± 0.53	NA	NA	NA	NA
Lu	ICP-MS	ppm	0.14 ± 0.03	0.27 ± 0.11	0.29 ± 0.10	0.27 ± 0.07	0.18 ± 0.05	0.24 ± 0.05	0.28 ± 0.05	0.33 ± 0.11	0.20 ± 0.05	0.23 ± 0.05	0.42 ± 0.27	0.40 ± 0.13	NA	NA	NA	NA

Notes: [a]Average ± standard deviation of the number (*n*) indicated. [b]OC1, OC2, OC3, and OC4 are organic carbon produced at 120, 250, 450, and 550 °C, respectively, in a He atmosphere; EC1, EC2, and EC3 are elemental carbon produced at 550, 700, and 800 °C, respectively, in a 2% O$_2$/98% He atmosphere; OP is the pyrolyzed carbon fraction, determined when reflected laser light attained its original intensity after O$_2$ was added to the combustion atmosphere; CO$_3$-C was measured as carbon by acidification of sample. [c]AAS = atomic absorption spectrophotometry, AC = automatic colorimeter, IC = ion chromatography, ICP-MS = inductively coupled plasma-mass spectrometry, XRF = X-ray fluorescence spectrometry, NA = not analyzed, ppm = parts per million.
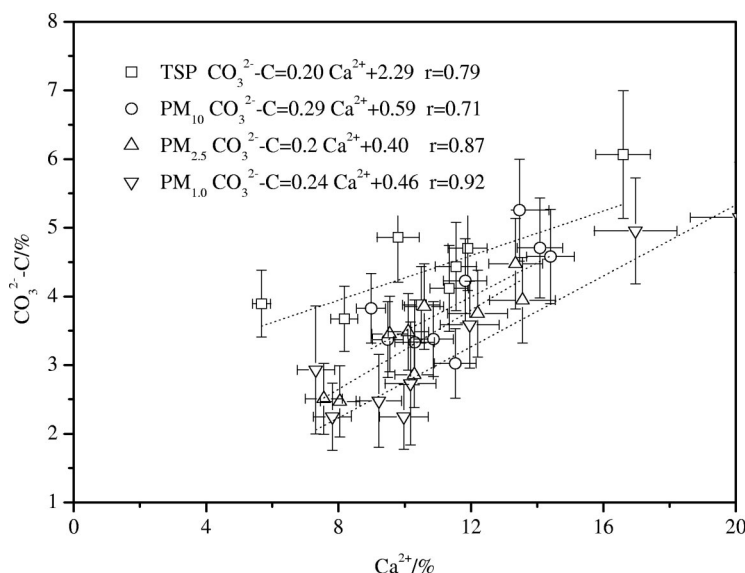
Figure 2. Relationship between carbonate carbon (CO_3^{2-}-C) and water-soluble calcium (Ca^{2+}) for the TSP, PM_{10}, $PM_{2.5}$, and PM_1 fractions of loess.

upper crust. The use of UCC as a reference to represent pure or paleo Asian dust needs to be further evaluated.

Comparisons with Dust-Dominated Ambient Measurements in Source Regions

Table 3 compares elemental ratios from these samples with those measured in other Chinese source regions.[14–16,18–21] The ratios of crustal elements such as Mg, Si, Fe, Ti, Mn, and Sr to Al in ambient samples are similar to those of PM loess. Ca/Al ratios varied from 1.8 ± 0.25 to 2.3 ± 0.12 for the loess samples, but their variability is

higher in the ambient samples. The ambient Ca/Al ratio from the Taklimakan Desert is approximately 40% higher than the average ratios in PM loess, and they are 50–80% lower for the other samples.

Major differences between loess and ambient sample ratios are evident for species that might originate from other sources (e.g., K, P, V, Cr, Cu, Zn, Ni, and Pb). The K to Al ratio is 40–200% higher in ambient air than in PM loess. Figure 4 shows the anthropogenic fraction of disturbed or contaminated elements for $PM_{2.5}$ of ZBT dust aerosol reported by Arimoto et al.[9] More than 70% of Pb,
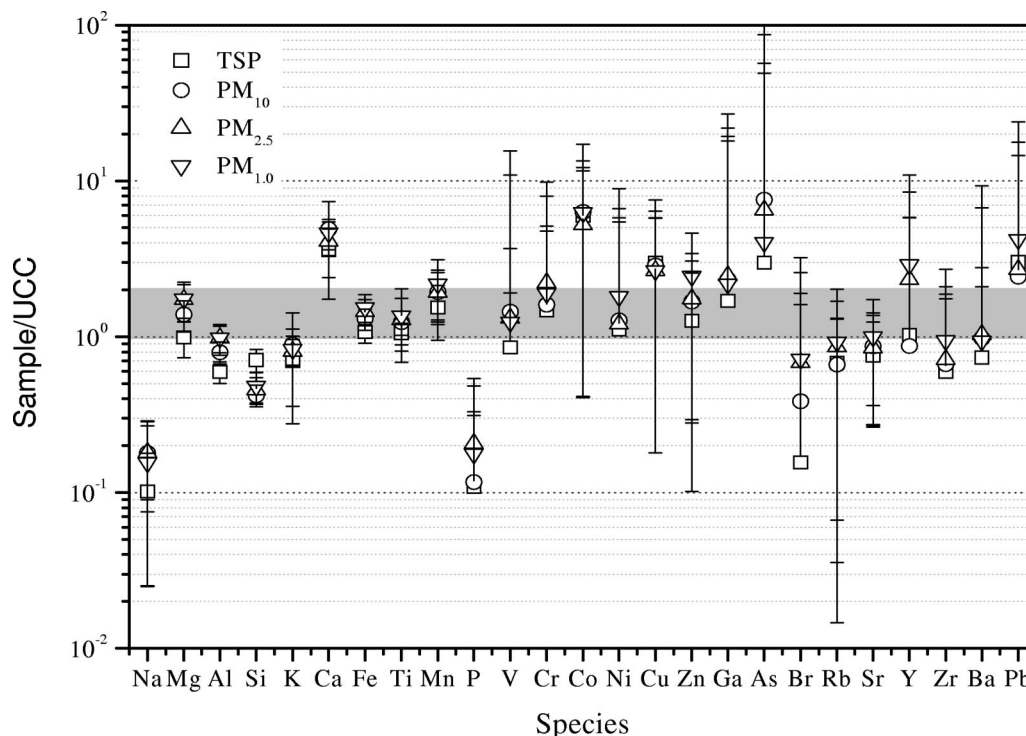
Figure 3. UCC[55]-normalized abundances for TSP, PM_{10}, $PM_{2.5}$, and PM_1 of loess. Samples for each size fraction represent the average of nine source profiles.

Table 3. Comparison of elemental ratios (uncertainties) for loess PM and dust-dominated aerosol in source regions.

| Size fractions | CLP | | | | Mu Us Desert | | Tenggeli Desert | | Takalamagan Desert | | Hunshan Daka Sand-Land | | Horqin Sand-Land |
| | Xi Feng[a] | Xi Feng[a] | Xi Feng[a] | Xi Feng[a] | Zhenbeitai[20] | Zhenbeitai[14] | Zhenbeitai[19] | Zhenbeitai[15] | Shapotou[20] | Aksu[21] | Sunite Zuoqi[16] | Sanggen Dalai[16] | Tongliao[18] |
	TSP (n = 9)	PM$_{10}$ (n = 9)	PM$_{2.5}$ (n = 9)	PM$_1$ (n = 9)	TSP (n = 58)	PM$_9$ (n = 24)	PM$_{2.5}$	PM$_{2.5}$ (n = 22)	TSP (n = 1)	TSP (n = 18)	TSP	TSP	PM$_{2.5}$
Mg/Al	0.28 (0.08)	0.29 (0.08)	0.29 (0.09)	0.29 (0.11)	0.31	0.32 (0.03)	0.28	0.35	NA	0.48	0.31	0.25	0.19
Si/Al	4.56 (1.05)	2.03 (0.46)	1.79 (0.49)	1.88 (0.59)	4.18	2.79 (0.04)	NA	1.9	2.37	4.18	NA	NA	4.06
K/Al	0.41 (0.25)	0.39 (0.24)	0.29 (0.08)	0.29 (0.09)	0.27	0.31 (0.02)	0.56	0.32	0.51	0.52	0.8	0.47	0.44
Ca/Al	2.25 (0.2)	2.29 (0.12)	1.56 (0.24)	1.77 (0.25)	0.86	0.79 (0.15)	0.92	1	1.95	2.05	0.4	0.53	0.76
Fe/Al	0.69 (0.03)	0.65 (0.01)	0.71 (0.02)	0.79 (0.07)	0.52	0.63 (0.04)	0.71	0.59	0.78	1	1.07	1.03	0.78
Ti/Al	0.052	0.048	0.058	0.067 (0.005)	0.078	0.054 (0.004)	0.08	0.051	0.096	0.086	0.12	0.078	0.063
Mn/Al	0.02 (0.002)	0.015 (0.002)	0.018 (0.002)	0.02 (0.002)	0.014	0.015 (0.002)	0.027	0.015	0.012	0.017	0.02	0.019	0.02
P/Al	0.0016 (0.001)	0.0019 (0.002)	0.0012 (0.001)	0.0015 (0.001)	0.096	0.013	NA	NA	NA	0.085	NA	NA	0.05
V/Al	0.001 (0.004)	0.001 (0.002)	0.001 (0.001)	0.001 (0.0007)	0.0007	NA	0.0027	0.011	0.005	0.001	0.0036	0.0036	0.01
Cr/Al	0.0009 (0.001)	0.001 (0.0009)	0.0009 (0.0007)	0.001 (0.0008)	0.001	NA	0.0017	0.019	NA	0.0017	NA	NA	0.01
Co/Al	0.0003 (0.00008)	0.0002 (0.00004)	0.0003 (0.00004)	0.0002 (0.00005)	NA	NA	NA	0.0008	0.016	NA	NA	NA	NA
Ni/Al	0.0007 (0.0002)	0.0007 (0.0002)	0.0008 (0.0005)	0.0006 (0.0001)	0.0062	NA	NA	0.003	0.0063	0.0075	0.0012	0.0053	0.003
Cu/Al	0.0009 (0.0004)	0.0016 (0.001)	0.0018 (0.002)	0.001 (0.001)	0.0034	NA	0.001	0.0062	0.012	0.0037	0.0027	0.0016	0.01
Zn/Al	0.0016 (0.001)	0.002 (0.001)	0.0016 (0.001)	0.003 (0.004)	NA	NA	0.0098	0.035	0.01	0.0018	0.004	0.0055	0.09
Rb/Al	0.0016 (0.0004)	0.0015 (0.0003)	0.0015 (0.0002)	0.0014 (0.0003)	NA	NA	NA	NA	NA	NA	NA	NA	NA
Sr/Al	0.0039 (0.002)	0.0032 (0.0006)	0.0037 (0.0008)	0.0035 (0.001)	NA	NA	0.006	0.005	NA	NA	NA	NA	NA
Zr/Al	0.0023 (0.0014)	0.0017 (0.001)	0.002 (0.0015)	0.002 (0.0015)	NA	NA	NA	NA	NA	NA	NA	NA	NA
Ba/Al	0.0065 (0.019)	0.0073 (0.013)	0.0084 (0.005)	0.0085 (0.006)	NA	NA	0.011	0.009	NA	NA	NA	NA	NA
Pb/Al	0.0005 (0.0002)	0.0005 (0.0002)	0.0005 (0.0001)	0.0004 (0.0001)	0.01	NA	0.007	0.025	0.005	0.0057	0.0022	0.0079	0.02

Notes: [a]Samples collected during this study. NA = not analyzed.
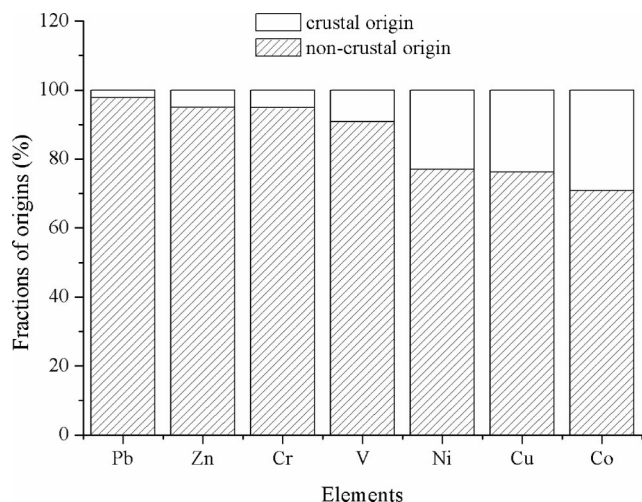
Figure 4. The percentages of crustal and non-crustal origin for elements Pb, Zn, Cr, V, Ni, Cu, and Co of $PM_{2.5}$ aerosol samples acquired from the ZBT station.[15] The fraction of non-crustal origin ($f_{\text{non-crustal origin}}$, in percent) for element X was calculated as follows: $f_{\text{non-crustal origin}} = 100 \times [1 - (Al_{\text{sample}} \times X_{\text{loess}})/(Al_{\text{loess}} \times X_{\text{sample}})]$.

Zn, Cr, V, Ni, Cu, and Co in ZBT aerosol were attributed to non-crustal or anthropogenic origins. Contributions from non-loess sources are most apparent for Pb (97%), followed by Zn (95%), Cr (94.7%), V (91%), Ni (77%), Cu (76%), and Co (70%). These results indicate that anthropogenic activities may have disturbed or contaminated the chemical components of aerosol in the source regions. The modern aerosol samples from the geological source-dominated environment are therefore not a "pure" soil product as compared with loess.

CONCLUSIONS

The chemical composition of Asian paleo dust derived from the CLP is similar throughout the past 198,000 yr in geological time. The elements Si, Ca, Al, Fe, K, Mg, Ca^{2+}, OC, and CC are the major constituents (>1%) in loess among the four PM fractions (i.e., TSP, PM_{10}, $PM_{2.5}$, and PM_1). Much of the calcium is water-soluble and corresponds with measures of carbonate, indicating that most Ca is in the form of $CaCO_3$ rather than other calcium minerals. Most of the K is insoluble, indicating that loess can be separated from biomass burning contributions when K^+ is measured. The loess has elemental abundances similar to those of the UCC for Mg, Fe, Ti, Mn, V, Cr, and Ni, but substantially different ratios for other elements (e.g., Ca, Co, Cu, As, and Pb), suggesting that the use of UCC as a reference to represent pure or paleo Asian dust needs to be further evaluated. The aerosol samples from the source regions have similar ratios to loess for Mg, Si, Fe, Ti, Mn, and Sr to Al, but substantially different ratios for species that might originate from anthropogenic sources (e.g., K, P, V, Cr, Cu, Zn, Ni, and Pb), indicating that the aerosol samples from the geological source-dominated environment are not a "pure" soil product as compared with loess.

As a natural atmospheric aerosol, dust plays an essential role on the regional and global climate and environmental changes.[8–13] Attempts have been made to simulate global dust distributions in several models.[57] Size-differentiated chemical characteristics of loess based on aerodynamic diameters reproduce the chemical characteristics of Asian paleo dust, which are valuable for reducing uncertainty in the evaluation of the role of Asian dust in climate and environmental change of geological times as well as in the modern period.

REFERENCES
1. Liu, T.S. *Loess and the Environment*; China Ocean Press: Beijing, People's Republic of China, 1985.
2. Duce, R.A.; Unni, C.K.; Ray, B.J.; Prospero, J.M.; Merrill, J.T. Long-Range Atmospheric Transport of Soil Dust from Asia to the Tropical North Pacific: Temporal Variability; *Science* **1980**, *209*, 1522-1524.
3. Jaffe, D.; Snow, J.; Cooper, O. The 2001 Asian Dust Events: Transport and Impact on Surface Aerosol Concentrations in the U.S.; *EOS Trans. AGU* **2003**, *84*, 501-516.
4. Biscaye, P.E.; Grousset, F.E.; Revel, M.; Van der Gaast, S.; Zielinski, G.A.; Vaars, A.; Kukla, G. Asian Provenance of Glacial Dust (Stage 2) in the Greenland Ice Sheet Project 2 Ice Core, Summit, Greenland; *J. Geophys. Res.* **1997**, *102*, 765-781.
5. Grousset, F.E.; Ginoux, P.; Bory, A.; Biscaye, P.E. Case Study of a Chinese Dust Plume Reaching the French Alps; *Geophys. Res. Lett.* **2003**, *30*, 10-1-10-4.
6. Qiang, X.K.; Li, Z.X.; Powell, C.; Zheng, H.B. Magneto-Stratigraphic Record of the Late Miocene Onset of the East Asia Monsoon, and Pliocene Uplift of Northern Tibet; *Earth Planet. Sci. Lett.* **2001**, *187*, 83-93.
7. Guo, Z.T.; Ruddiman, W.F.; Hao, Q.Z.; Wu, H.B.; Qiao, Y.S.; Zhu, R.X.S.; Peng, Z.; Wei, J.J.; Yuan, B.Y.; Liu, T.S. Onset of Asian Desertification by 22 MYR Ago Inferred from Loess Deposits in China; *Nature* **2002**, *416*, 159-163.
8. *IPCC Climate Change 2007: The Physical Science Basis. Summary for Policymakers. Contribution of Working Group I to the Fourth Assessment Report of the Intergovernmental Panel on Climate Change*; Intergovernmental Panel on Climate Change (IPCC): Geneva, Switzerland, 2007; available at *http://www.ipcc.ch/SPM2feb07.pdf* (accessed 2007).
9. Chadwick, O.A.; Derry, L.A.; Vitousek, P.M.; Huebert, B.J.; Hedin, L.O. Changing Sources of Nutrients during Four Million Years of Ecosystem Development; *Nature* **1999**, *397*, 491-497.
10. Swap, R.; Garstang, M.; Greco, S.; Talbot, R.; Kallberg, P. Saharan Dust in the Amazon Basin; *Tellus* **1992**, *44*, 133-149.
11. Jickells, T.D.; An, Z.S.; Andersen, K.K.; Baker, A.R.; Bergametti, G.; Brooks, N.; Cao, J.J.; Boyd, P.W.; Duce, R.A.; Hunter, K.A.; Kawahata, H.; Kubilay, N.; laRoche, J.; Liss, P.S.; Mahowald, N.; Prospero, J.M.; Ridgwell, A.J.; Tegen, I.; Torres, R. Global Iron Connections between Desert Dust, Ocean Biogeochemistry and Climate; *Science* **2005**, *308*, 67-71.
12. Sokolik, I.N.; Toon, O.B. Incorporation of Mineralogical Composition into Models of the Radiative Properties of Mineral Aerosol from UV to IR Wavelengths; *J. Geophys. Res.* **1999**, *104*, 9423-9444.
13. Sokolik, I.N.; Winker, D.M.; Bergametti, G.; Gillette, D.A.; Carmichael, G.R.; Kaufman, Y.J.; Gomes, L.; Schuetz, L.; Penner, J.E. Introduction to Special Section: Outstanding Problems in Quantifying the Radiative Impacts of Mineral Dust; *J. Geophys. Res.* **2001**, *106*, 18015-18027.
14. Alfaro, S.C.; Gomes, L.; Rajot, J.L.; Lafon, S.; Gaudichet, A.; Chatenet, B.; Maille, M.; Cautenet, G.; Lasserre, F.; Cachier, H.; Zhang, X.Y. Chemical and Optical Characterization of Aerosols Measured in Spring 2002 at the ACE-Asia Supersite, Zhenbeitai, China; *J. Geophys. Res.* **2003**, *108*; doi: 10.1029/2002JD003214.
15. Arimoto, R.; Zhang, X.Y.; Huebert, B.J.; Kang, C.H.; Savoie, D.L.; Prospero, J.M.; Sage, S.K.; Schloesslin, C.A.; Khaing, H.M.; Oh, S.N. Chemical Composition of Atmospheric Aerosols from Zhenbeitai, China, and Gosan, South Korea, during ACE-Asia; *J. Geophys. Res.* **2004**, *109*, D19S04; doi: 10.1029/2003JD004323.
16. Cheng, T.T.; Lu, D.R.; Wang, G.C.; Xu, Y.F. Chemical Characteristics of Asian Dust Aerosol from Hunshan Dake Sandland in Northern China; *Atmos. Environ.* **2005**, *39*, 2903-2911.
17. Mori, I.; Nishikawa, M.; Quan, H.; Morita, M. Estimation of the Concentration and Chemical Composition of Kosa Aerosols at Their Origin; *Atmos. Environ.* **2002**, *39*, 4569-4575.

18. Shen, Z.X.; Cao, J.J.; Arimoto, R.; Zhang, R.J.; Jie, D.M.; Liu, S.X.; Zhu, C.S. Chemical Composition and Source Characterization of Spring Aerosol over Horqin Sand Land in Northeastern China; *J. Geophys. Res.* **2007**, *112*, D14315; doi: 10.1029/2006JD007991.

19. Xu, J.; Bergin, M.H.; Greenwald, R.; Schauer, J.J.; Shafer, M.M.; Jaffrezo, J.L.; Aymoz, G. Aerosol Chemical, Physical, and Radiative Characteristics near a Desert Source Region of Northwest China during ACE-Asia; *J. Geophys. Res.* **2004**, *109*, D19SO3; doi: 10.1029/2003JD004239.

20. Zhang, X.Y.; Arimoto, R.; An, Z.S.; Chen, T.; Zhang, G.; Zhu, G.; Wang, X. Atmospheric Trace Elements over Source Regions for Chinese Dust: Concentrations, Sources, and Atmospheric Deposition on the Loess Plateau; *Atmos. Environ.* **1993**, *27*, 2051-2067.

21. Zhang, X.Y.; Gong, S.L.; Shen, Z.X.; Mei, F.M.; Xi, X.X.; Liu, L.C.; Zhou, Z.J.; Wang, D.; Wang, Y.Q.; Cheng, Y. Characterization of Soil Dust Aerosol in China and Its Transport and Distribution during 2001 ACE-Asia: 1. Network Observations; *J. Geophys. Res.* **2003**, *108*; doi: 10.1029/2002JD002632.

22. Zhang, R.J.; Arimoto, R.; An, J.L.; Yabuki, S.; Sun, J.H. Ground Observations of a Strong Dust Storm in Beijing in March 2002; *J. Geophys. Res. Atmos.* **2005**, *110*, D18S06; doi: 10.1029/2004JD004589.

23. Nishikawa, M.; Quan, H.; Morita, M. Preparation and Evaluation of Certified Reference Materials for Asian Mineral Dust; *Global Environ. Res.* **2000**, *4*, 103-113.

24. Cao, J.J.; Chow, J.C.; Watson, J.G.; Wu, F.; Han, Y.M.; Jin, Z.D.; Shen, Z.X.; An, Z.S. Size-Differentiated Source Profiles for Fugitive Dust in the Chinese Loess Plateau; *Atmos. Environ.* **2008**, *42*, 2261-2275.

25. Cao, J.J.; Zhu, C.S.; Chow, J.C.; Liu, W.G.; Han, Y.M.; Watson, J.G. Stable Carbon and Oxygen Isotopic Composition of Carbonate in Fugitive Dust in the Chinese Loess Plateau; *Atmos. Environ.* **2008**, *42*, 9118-9122.

26. Chow, J.C.; Watson, J.G. Survey of Measurement and Composition of Ultrafine Particles. *AAQR* **2007**, *7*, 121-173.

27. An, Z.S.; Liu, T.S.; Lu, Y.C.; Porter, S.C.; Kukla, G.; Wu, X.H.; Hua, Y.M. The Long-Term Paleo-Monsoon Variation Recorded by the Loess-Paleosol Sequence in Central China; *Quat. Int.* **1990**, *718*, 91-95.

28. Zhang, X.Y.; Arimoto, R.; An, Z.S.; Chen, T.; Zhang, G.; Ray, B.J. Late Quaternary Records of the Atmospheric Input of Eolian Dust to the Center of the Chinese Loess Plateau; *Quat. Res.* **1994**, *41*, 35-43.

29. Gallet, S.; Jahn, B.-M.; Van Vliet. Lanoe, B.; Dia, A.; Rossello, E. Loess Geochemistry and Its Implications for Particle Origin and Composition of the Upper Continental Crust; *Earth Planet. Sci. Lett.* **1998**, *156*, 157-172.

30. Gallet, S.; Jahn, B.-M.; Torii, M. Geochemical Characterization of the Luochuan Loess-Paleosol Sequence, China, and Paleoclimatic Implications; *Chem. Geol.* **1996**, *133*, 67-88.

31. Chen, J.; An, Z.; Head, J. Variation of Rb/Sr in the Loess-Paleosol Sequences of Central China during the Last 130,000 Years and Their Implications for Monsoon Paleoclimatology; *Quat. Res.* **1999**, *51*, 215-219.

32. Chen, J.; Li, G.J.; Yang, J.D.; Rao, W.B.; Lu, H.Y.; Balsam, W.; Sun, Y.B.; Ji, J.F. Nd and Sr Isotopic Characteristics of Chinese Deserts: Implications for the Provenances of Asian Dust; *Geochim. Cosmochim. Acta* **2007**, *71*, 3904-3914.

33. Chen, J.; Chen, Y.; Liu, L.W.; Ji, J.F.; Balsam, W.; Sun, Y.B.; Lu, H.Y. Zr/Rb Ratio in the Chinese Loess Sequences and Its Implication for Changes in the East Asian Winter Monsoon Strength; *Geochim. Cosmochim. Acta* **2006**, *70*, 1471-1482.

34. Chow, J.C.; Watson, J.G.; Houck, J.E.; Pritchett, L.C.; Rogers, C.F.; Frazier, C.A.; Egami, R.T.; Ball, B.M. A Laboratory Resuspension Chamber to Measure Fugitive Dust Size Distributions and Chemical Compositions; *Atmos. Environ.* **1994**, *28*, 3463-3481.

35. Sun, Y.B.; An, Z.S. Late Pliocene-Pleistocene Changes in Mass Accumulation Rates of Eolian Deposits on the Central Chinese Loess Plateau; *J. Geophys. Res.* **2005**, *110*, D23101; doi: 10.1029/2005JD006064.

36. Martinson, D.G.; Pisias, N.; Hays, J.D.; Imbrie, J.; Moor, T.C., Jr.; Shackelton, N.J. Age Dating and the Orbital Theory of the Ice Ages: Development of a High-Resolution 0 to 300,000 Year Chronostratigraphy; *Quat. Res.* **1987**, *27*, 1-29.

37. Watson, J.G.; Chow, J.C.; Frazier, C.A. In *Elemental Analysis of Airborne Particles*, Vol. 1; Landsberger, S., Creatchman, M., Eds.; Gordon and Breach Science: Amsterdam, The Netherlands, 1999; pp 67-96.

38. Hutton, R.C.; Eaton, A.N. Role of Aerosol Water Vapour Loading in Inductively Coupled Plasma Mass Spectrometry; *J. Anal. At. Spectrom.* **1987**, *2*, 595-598.

39. Zhu, G.; Browner, R.F. Study of the Influence of Water Vapour Loading and Interface Pressure in Inductively Coupled Plasma Mass Spectrometry; *J. Anal. At. Spectrom.* **1988**, *3*, 781-789.

40. Ben-Younes, M.; Gregoire, D.C.; Chakrabarti, C.L. Effectiveness of Ammonia in Reducing Carbon-Based Polyatomic Ion Interferences in Electrothermal Vaporization Collision Cell Inductively Coupled Plasma Mass Spectrometry; *Spectrochim. Acta B* **2003**, *58*, 361-372.

41. Ingle, C.P.; Appelblad, P.K.; Dexter, M.A.; Reid, H.J.; Sharp, B.L. The Use of Background Ions and a Multivariate Approach to Characterise and Optimise the Dominant H_2-Based Chemistries in a Hexapole Collision Cell Used in ICP-MS; *J. Anal. At. Spectrom.* **2001**, *16*, 1076-1084.

42. Niemela, M.; Peramaki, P.; Kola, H.; Piispanen, J. Determination of Arsenic, Iron and Selenium in Moss Samples Using Hexapole Collision Cell, Inductively Coupled Plasma-Mass Spectrometry; *Anal. Chim. Acta* **2003**, *493*, 3-12.

43. Chow, J.C.; Watson, J.G. In *Elemental Analysis of Airborne Particles*, Vol. 1; Landsberger, S., Creatchman, M., Eds.; Gordon and Breach Science: Amsterdam, The Netherlands, 1999; pp 97-137.

44. Chow, J.C.; Watson, J.G.; Pritchett, L.C.; Pierson, W.R.; Frazier, C.A.; Purcell, R.G. The DRI Thermal/Optical Reflectance Carbon Analysis System: Description, Evaluation and Applications in U.S. Air Quality Studies; *Atmos. Environ.* **1993**, *27*, 1185-1201.

45. Chow, J.C.; Watson, J.G.; Chen, L.-W.A.; Arnott, W.P.; Moosmüller, H.; Fung, K.K. Equivalence of Elemental Carbon by Thermal/Optical Reflectance and Transmittance with Different Temperature Protocols; *Environ. Sci. Technol.* **2004**, *38*, 4414-4422.

46. Chow, J.C.; Watson, J.G.; Chen, L.-W.A.; Paredes-Miranda, G.; Chang, M.C.O.; Trimble, D.; Fung, K.K.; Zhang, H.; Yu, J.Z. Refining Temperature Measures in Thermal/Optical Carbon Analysis; *Atmos. Chem. Phys.* **2005**, *5*, 2961-2972.

47. Chow, J.C.; Watson, J.G.; Chen, L.-W.A.; Chang, M.C.O.; Robinson, N.F.; Trimble, D.; Kohl, S.D. The IMPROVE_A Temperature Protocol for Thermal/Optical Carbon Analysis: Maintaining Consistency with a Long-Term Database; *J. Air & Waste Manage. Assoc.* **2007**, *57*, 1014-1023; doi: 10.3155/1047-3289.57.9.1014.

48. Chow, J.C.; Watson, J.G. $PM_{2.5}$ Carbonate Concentrations at Regionally Representative IMPROVE Sites; *Geophys. Res. Atmos.* **2002**, *107*; doi: 10.1029/2001JD000574.

49. Watson, J.G.; Chow, J.C. Source Characterization of Major Emission Sources in the Imperial and Mexicali Valleys along the U.S./Mexico Border; *Sci. Total Environ.* **2001**, *276*, 33-47.

50. Watson, J.G. Visibility: Science and Regulation—2002 Critical Review; *J. Air & Waste Manage. Assoc.* **2002**, *52*, 628-713.

51. Chow, J.C.; Watson, J.G.; Ashbaugh, L.L.; Magliano, K.L. Similarities and Differences in PM_{10} Chemical Source Profiles for Geological Dust from the San Joaquin Valley, California; *Atmos. Environ.* **2003**, *37*, 1317-1340.

52. Chow, J.C.; Watson, J.G.; Kuhns, H.D.; Etyemezian, V.; Lowenthal, D.H.; Crow, D.J.; Kohl, S.D.; Engelbrecht, J.P.; Green, M.C. Source Profiles for Industrial, Mobile, and Area Sources in the Big Bend Regional Aerosol Visibility and Observational (BRAVO) Study; *Chemosphere* **2004**, *54*, 185-208.

53. Watson, J.G.; Chow, J.C.; Houck, J.E. $PM_{2.5}$ Chemical Source Profiles for Vehicle Exhaust, Vegetative Burning, Geological Material, and Coal Burning in Northwestern Colorado during 1995; *Chemosphere* **2001**, *43*, 1141-1151.

54. Cao, J.J.; Lee, S.C.; Zhang, X.Y.; Chow, J.C.; An, Z.S.; Ho, K.F.; Watson, J.G.; Fung, K.K.; Wang, Y.Q.; Shen, Z.X. Characterization of Airborne Carbonate over a Site near Asian Dust Source Regions during Spring 2002 and Its Climatic and Environmental Significance; *J. Geophys. Res. Atmos.* **2005**, *110*, 1-8; doi: 10.1029/2004JD005244.

55. Taylor, S.R.; MacLennan, S.M. The Geochemical Evolution of the Continental Crust; *Rev. Geophys.* **1995**, *33*, 241-165.

56. Wang, Y.Q.; Zhang, X.Y.; Arimoto, R.; Cao, J.J.; Shen, Z.X. Characteristics of Carbonate Content and Carbon and Oxygen Isotopic Composition of Northern China Soil and Dust Aerosol and Its Application to Tracing Dust Sources; *Atmos. Environ.* **2005**, *39*, 2631-2642.

57. Mahowald, N.; Kohfeld, K.E.; Hansson, M.; Balkanski, Y.; Harrison, S.P.; Prentice, I.C.; Schulz, M.; Rodhe, H. Dust Sources and Deposition during the Last Glacial Maximum and Current Climate: A Comparison of Model Results with Palaeodata from Ice Cores and Marine Sediments; *J. Geophys. Res.* **1999**, *104*, 15895-15916.

About the Authors

Dr. Feng Wu is an assistant professor and Junji Cao and Zhisheng An are professors at the Institute of Earth Environment of the Chinese Academy of Sciences. Judith C. Chow and John G. Watson are research professors at DRI, Nevada System of Higher Education, Reno, NV. Please address correspondence to: Dr. Feng Wu, Institute of Earth Environment, Chinese Academy of Sciences, Xi'an, 710075, People's Republic of China; phone: +86-29-88316017; fax: +86-29-88320456; e-mail: kurt_wf@ieecas.cn.